Single Atoms Anchored in Hexagonal Boron Nitride for Propane Dehydrogenation from First Principles

Chuanye Xiong[a,b], Prof. Dr. Sheng Dai[c,d], Dr. Zili Wu[c,e], Prof. Dr. De-en Jiang[a,b]*

[a]Department of Chemical and Environmental Engineering, University of California, Riverside, California 92521, United States

[b]Department of Chemistry, University of California, Riverside, California 92521, United States

[c]Chemical Sciences Division, Oak Ridge National Laboratory, Oak Ridge, Tennessee 37831, United States

[d]Department of Chemistry, The University of Tennessee, Knoxville, Tennessee 37996, United States

[e]Center for Nanophase Materials Sciences, Oak Ridge National Laboratory, Oak Ridge, Tennessee 37831, United States

*djiang@ucr.edu (twitter: @DeenJiang)

Website: https://nanochem.ucr.edu

Abstract

Single-atom catalysts embedded in N-doped graphene have attracted great interest recently, but the hexagonal boron nitride (h-BN) is much less explored as a support. Using first principles density function theory and molecular dynamics, here we investigate the stability of Pt, Au, and Ru single atoms anchored at B and N vacancies on h-BN. We find that Pt and Ru single atoms are much more stable than Au on h-BN. We further examine propane dehydrogenation on these single-atom catalysts and find that Pt_1 at the B vacancy in h-BN and Ru_1 at the N vacancy in h-BN show excellent activity for propane dehydrogenation, as evidenced by low energy barriers for both dehydrogenation steps. Our work suggests that Pt and Ru single atoms anchored at vacancy sites in h-BN could be promising for propane dehydrogenation.

Introduction

Single atom catalysis has attracted great interest in heterogeneous catalysis in the past decade.[1] Doped graphene is a widely used substrate to support metal single atoms due to the excellent metal-support interaction,[2] high specific surface area,[3] and high electron conductivity.[4] For example, it was found that the FeN_4 center and the N-group in graphene can enhance oxygen reduction reaction,[5] while Co single atoms on N-doped graphene show high activity and stability in hydrogen evolution reaction.[6]

As two prototypical 2D materials, graphene and hexagonal boron nitride (h-BN) share many properties. Hence, h-BN can be a potential candidate for anchoring single atoms, especially at high temperatures due to its high thermal stability. In fact, Hermans and co-workers reported that boron nitride itself is an excellent catalyst for alkane oxidative dehydrogenation with a high propene selectivity.[7-8] Moreover, Uosaki et al. found that the interface between Au(111) and boron nitride nanosheet can promote oxygen reduction reaction.[9] Researchers also were able to resolve defect sites in boron nitride.[10] Dai and coworkers synthesized ultrathin h-BN sheets with plenty of vacancies sites and found that the h-BN supported Pt nanoparticles have higher activity for CO oxidation than silica-supported Pt.[11-12]

Although h-BN-supported single atoms have not been reported experimentally, researchers have computationally examined them for catalytic reactions, such as CO oxidation.[13-18] More interestingly, Zhao and Chen predicted that h-BN-supported Mo single atom is a potential catalyst for electrocatalytic N_2 reduction,[19] while Deng et al. suggested that Co embedded in h-BN may be promising for oxygen reduction reaction.[20] One thing to note is that these studies focused on only the B vacancy, but N vacancy has been observed experimentally in h-BN as well.[21]

Recently the h-BN nanosheets have also been explored as a support for Pt nanoparticles[22] and Pt/Cu nanoclusters[23] for direct dehydrogenation of propane on a

benchtop scale. Oxide-supported Pt nanoparticles are used commercially in direct dehydrogenation of propane[24] which has been subject to a plethora of experimental studies. It has been shown that Pt exists as nanoclusters of 15 – 25 atoms on the oxide support.[25] Owing to its high surface area and good thermal stability, γ-Al_2O_3 is the most commonly used support for Pt nanoparticles, but its acid sites can contribute to coke formation.[26] Therefore, alloying elements such as Sn have been used to form intermetallic nanoparticles with Pt to avoid coking.[24] Moreover, Pt single atoms have been observed together with larger clusters on oxide support,[25] prompting the speculation that they might be able to catalyze propane dehydrogenation (PDH).[24] Indeed, recent studies have demonstrated the excellent performance of Pt single atoms for PDH, either as single-atom alloys on oxides[27] or isolated atoms anchored in dealuminated zeolite.[28]

The experimental findings of Pt single atoms for PDH have inspired many recent computational studies in exploring Pt single atoms for PDH beyond the oxide supports. Density function theory calculations predicted that single atom Pt on N-doped graphene enhances the Pt's activity in direct dehydrogenation of propane.[29] On the other hand, using Pt single atoms can maximize atomic efficiency[1] and boost turnover.[30] In addition to Pt,[1, 31] Au,[32-33] and Ru[34-35] are also popular single-atom systems. When combined with a thermally stable support such as h-BN, these SACs may offer attractive advantages for dehydrogenation of propane, especially in anti-coking and in improving the turnover frequency per Pt atom, as coke formation[36] is a known problem for the conventional Pt/alumina catalyst where Pt exists as nanoclusters of 15 – 25 atoms.[25] Answering these questions computationally can help guide the experimental discovery of h-BN-supported single atoms for PDH. Hence, herein we investigate from first principles the stability of these single atoms anchored on both N and B vacancies on h-BN and their activity for propane dehydrogenation. Below we first present the stability results of SACs on h-BN, and then show their PDH energetics. We further explain the trend from the analyses of partial charges, d-band center, and density of states.

Results and Discussion

Static stability of Pt, Au, and Ru single atoms on h-BN

Since stability is a critical factor for assessing a catalyst, we first examine the stability of Pt, Au, and Ru single atoms on B/N vacancy sites of the h-BN support. Their optimized structures are shown in Figure 1. One can see that the single atom is slightly above the plane of h-BN. Judging from the distances of the single atoms to their first coordination shell and their height above the h-BN plane (Table 1), one can conclude that on the B vacancy Ru has the closest interaction with h-BN and Au the least; on the N vacancy, Au still has the least interaction. The anchoring energies of the single atoms indeed confirm this interaction trend (Figure 2): Ru has the strongest binding at the B vacancy and Pt the strongest at the N vacancy, while Au has the weakest binding at both vacancies. In addition, Ru's binding at the N vacancy is also very strong and only slightly weaker than that of Pt.

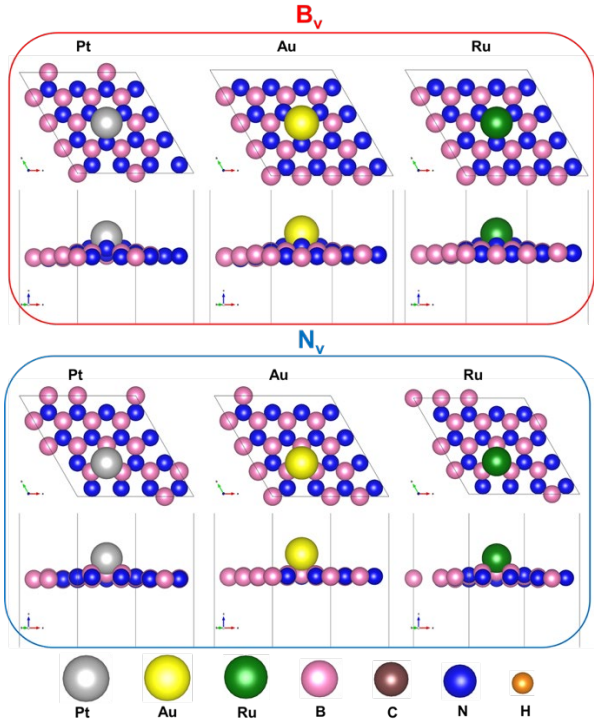

Figure 1. DFT-optimized structures of Pt, Au and Ru single atoms anchored on B vacancy (top) and N vacancy (bottom) on h-BN.

Table 1. The average M-N (r_{M-N}) distance at the B vacancy and M-B (r_{M-B}) distance at the N vacancy and the height (h) of the single atom M above the h-BN plane in the DFT optimized structures (h was calculated by the height of single atom minus the lowest atom in the substrate).

M	B_v		N_v	
	r_{M-N} (Å)	h (Å)	r_{M-B} (Å)	h (Å)
Pt	1.97	1.89	2.02	1.81
Au	2.06	2.08	2.27	2.00
Ru	1.92	1.77	2.01	1.91

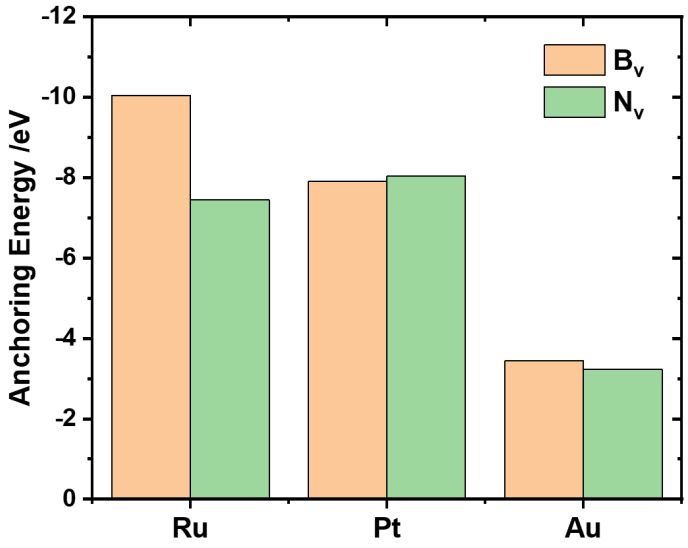

Figure 2. Anchoring energy of Pt, Au and Ru single atoms at the B and N vacancies on h-BN.

Dynamic stability of Pt, Au, and Ru single atoms on h-BN

To further examine the dynamic stability of the anchored single atoms, FPMD simulations were carried out at 1000 K to monitor the interaction between the single atoms and h-BN vacancies. As shown in Figure 3, both Ru and Pt single atoms are more stable at both types of vacancy sites on h-BN than their Au counterparts: the M-B or M-N distances vary within the range of 1.9 to 2.1 Å for Ru and Pt. Au is more stable on the B vacancy than on the N vacancy where the Au-B bond length varies a great deal, from 2.2 to 2.8 Å. The Au-N bond-length at the B vacancy varies from 2.0 to 2.3 Å. In addition, we find that adsorption of C_3H_8 negligibly impact the stability of the single atoms on the vacancy sites (Figure S2 in SI).

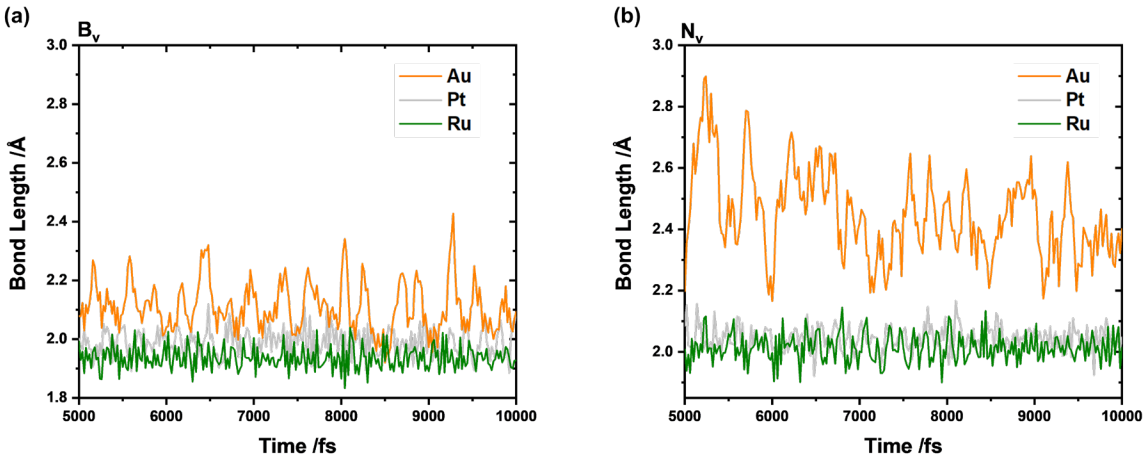

Figure 3. Changes in average bond lengths of the single atom (Pt/Au/Ru) to its three nearest N or B atoms on h-BN with time: (a) single atom at the B vacancy; (b) single atom at the N vacancy.

Chemical bonding of Pt, Au, and Ru single atoms on h-BN

To gain a deeper insight into the nature of the chemical bond between the Pt/Au/Ru single atom and the local environment on h-BN, we analyzed the crystal orbital Hamilton population (COHP) for one M-N bond at the B vacancy and one M-B bond at the N vacancy, which partitions the orbital overlapping between two atoms into bonding and antibonding states. The negative -COHP value refers to antibonding states while positive value refers to bonding states. As can be seen in Figure 4, both Au-B and Au-N bonds have the most antibonding population below and near the Fermi level, consistent with the weakest binding of Au with h-BN among the three metals. The integrated crystal orbital Hamilton population (ICOHP) up to the Fermi level provides a quantitative measure of the bonding vs antibonding population: the more negative the ICOHP value, the stronger the bonding. Indeed, one can see the overall correlation between the ICOHP values and the anchoring energy of the single atoms on h-BN (Figure 5). If we compare just Au at B_V and Au at N_V, then the correlation is not good. We think that this is mainly due to the very weak interaction between Au and the defected BN. In other words, because the interaction of Au with h-BN is very weak at both B_V and N_V, variation in ICOHP is not significant enough to differentiate the two sites.

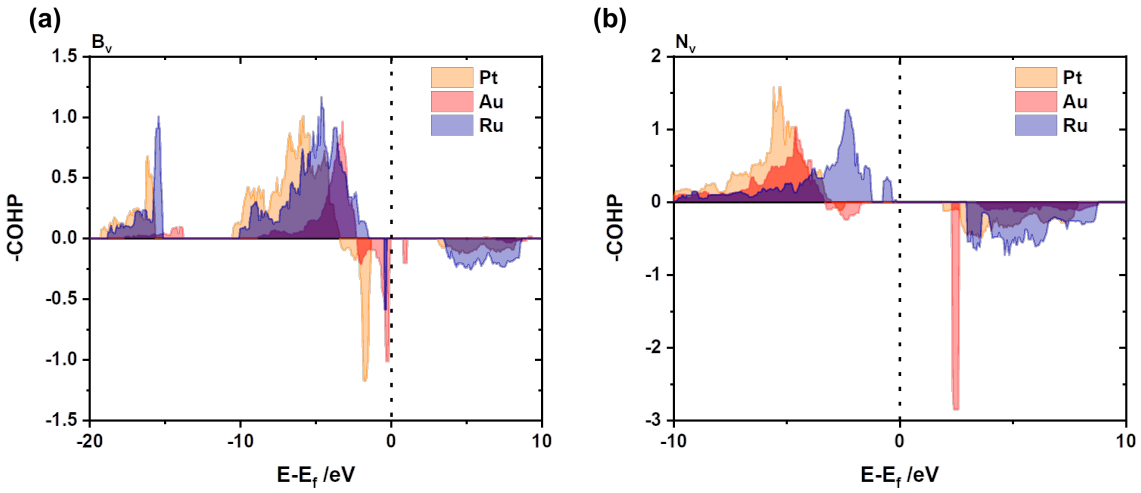

Figure 4. Crystal orbital Hamilton population (COHP) analysis of the single atom metal and adjacent N/B atom (E_f denoting the energy of the Fermi level): (a) at the B vacancy; (b) at the N vacancy.

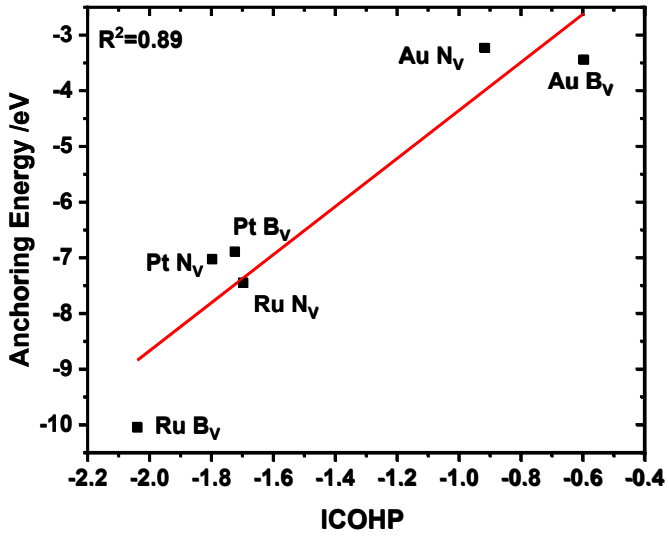

Figure 5. Correlation of the Pt/Au/Ru single-atom (M) anchoring energy on the B vacancy (B_V) and N vacancy (N_V) of h-BN with the corresponding integrated crystal orbital Hamilton population (ICOHP) of the M-N and M-B bonds.

We further examined the partial atomic charges of the Pt/Au/Ru single atoms by Bader analysis[37] and found that they are positively charged at the B vacancy but negatively charged at the N vacancy. This is consistent with the electronegativity trend: at the B vacancy, the metal atom is coordinated by the more electronegative N atoms, so loses some of its electrons; at the N vacancy, the metal atom is coordinated by the less electronegative

B atoms and gains some electrons. Moreover, Pt is most negative at the N vacancy site, while Ru is most positive at the B vacancy site.

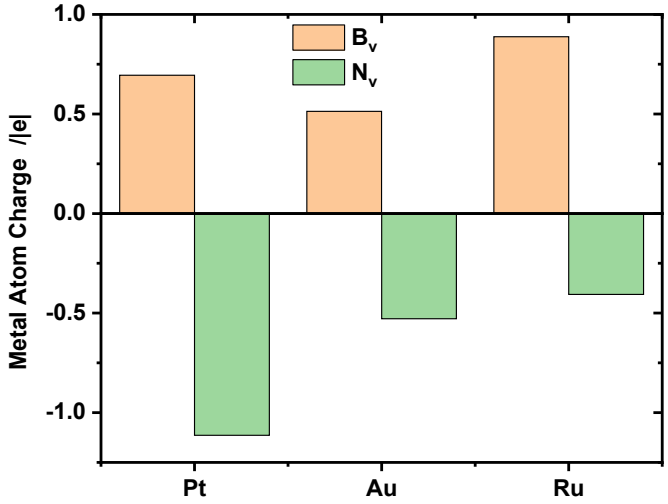

Figure 6. Bader charges of the Pt, Au and Ru single atoms anchored at the B vacancy (B_V) and N vacancy (N_V) sites of h-BN.

Propane dehydrogenation activity of the single atom on h-BN

To explore the potential of the M_1-h-BN for catalysis, we chose propane dehydrogenation as a test reaction. Figure 7 shows the energetic profiles and the corresponding key structures during the reaction pathways. The reaction can be divided into three key steps: i. C-H activation at the center carbon; ii. Second dehydrogenation at a terminal carbon; iii. Desorption of H_2 and C_3H_6. For M_1 anchored at the B vacancy (Figure 7a), Pt is the most active; for M_1 anchored at the N vacancy (Figure 7c), Ru is the most active, for both dehydrogenation steps. We note that the first dehydrogenation step of propane has a barrier of 0.51 eV at Pt_1-B_V-h-BN; for comparison, the barrier is 0.70 eV on Pt(111)[38] and 0.81 eV on Ru_1-N_V-h-BN. In addition, the intermediate states and transition states are similar on Pt_1-B_V-h-BN (Figure 7b) and Ru_1-N_V-h-BN (Figure 7d): C_3H_8 adsorbs on M_1; then C-H cleaves at TS1, leading to CH_3CHCH_3 and H co-adsorbed on M_1; next, second C-H cleaves at TS2, leading to CH_2CHCH_3 (propene) and 2H co-adsorbed on M_1; then, 2H

desorbs as H_2, followed by propene desorption. Figures S3 and S4 show more detailed structural comparison of TS1 for M_1-B_V-h-BN and M_1-N_V-h-BN. Because propane dehydrogenation usually takes place at high temperatures about 900 K,[24] desorption steps should not be a main concern here. But Au single atom is unlikely to survive such high temperature, considering its anchoring energy and stability (Figures 2 and 3).

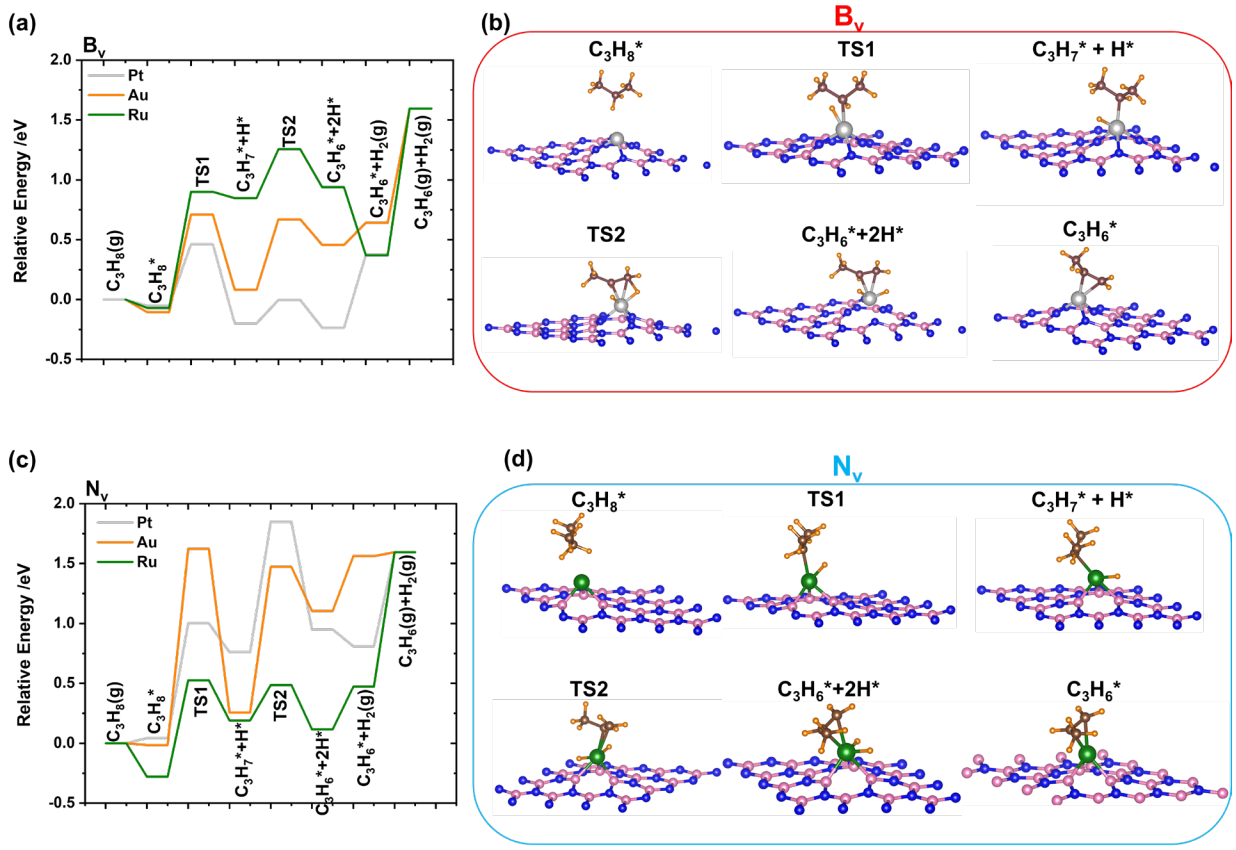

Figure 7. Propane dehydrogenation energy profile and the corresponding structures along the pathway: (a) energy profiles for M_1-B_V-h-BN; (b) structures for Pt_1-B_V-h-BN; (c) energy profiles for M_1-N_V-h-BN; (d) structures for Ru_1-N_V-h-BN.

As shown in Figure 7, the first C-H cleavage and the corresponding activation energy at TS1 are key to propane dehydrogenation. Overall, E_a at TS1 follows the Bell–Evans–Polanyi (BEP) principle: the more favorable the reaction energy (ΔE) is, the lower the activation energy. The only exception is Au_1-N_V-h-BN where E_a is the greatest (~1.6 eV) despite a slightly positive ΔE (~0.25 eV). To understand this exception of Au_1-N_V-h-BN,

we have compared its d-band center with others (Figure 8). One can see that there is a large down shift in the d-band center of Au_1 in Au_1-N_V-h-BN at TS1 (Figure 8b), meaning that Au_1 becomes much less reactive during the C-H cleavage process, which we think is the reason for its greatest E_a.

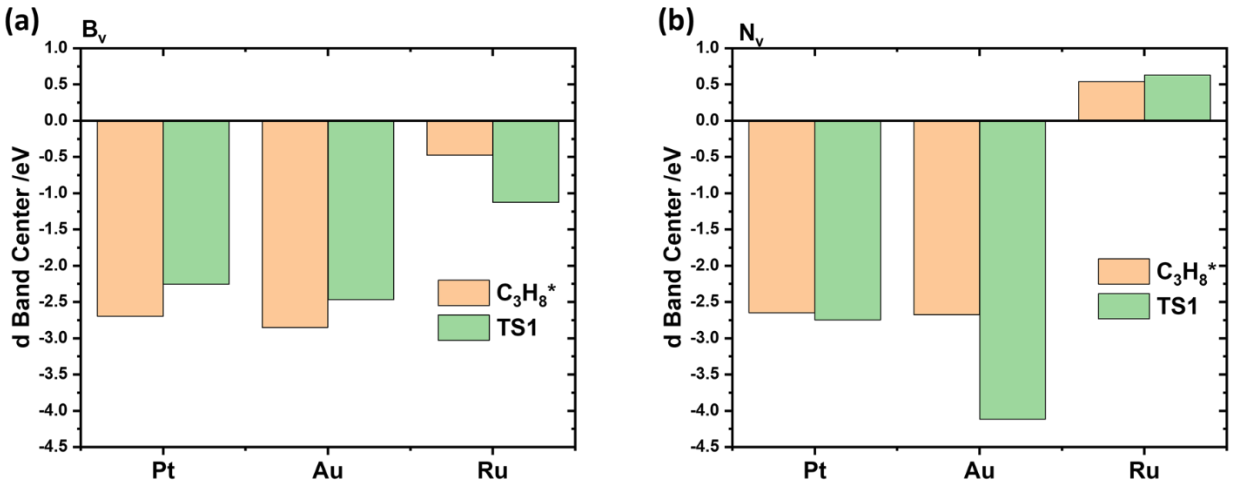

Figure 8. The center of the d-band of the metal single atom in the C_3H_8-adsorbed state (C_3H_8*) and at the transition of the first C-H cleavage (TS1): (a) Pt_1-B_V-h-BN; (b) M_1-N_V-h-BN.

3.5 Further considerations for experimental relevance

Although Pt_1 at the B vacancy and Ru_1 at the N vacancy of h-BN show great promise for PDH, factors such as sintering, coke formation, and desorption of propylene may negatively impact their experimental realization. Computationally, the sintering question can be addressed by examining the relative stability of metal clusters vs a single atom on defected h-BN, while the susceptibility to coke formation can be addressed by investigating the kinetics of further dehydrogenation tendencies and subsequent formation of aromatic compounds. The importance of propylene desorption is best addressed by microkinetic analysis of the whole PDH pathways. Further studies are warranted.

Conclusions

We have investigated the stability and propane dehydrogenation reactivity of Pt, Au and Ru singles atoms anchored at vacancy sites of h-BN from first principles DFT calculations. We found that the stability of Au single atom is much lower than that of Pt or Ru. The stability has been correlated to the integrated crystal orbital Hamilton population value, while Bader analysis showed opposite charges on the single atom for B vacancy vs N vacancy as the anchoring site. From the minimum-energy paths of propane dehydrogenation on these single-atom catalysts, we found that Pt_1 at the B vacancy in h-BN and Ru_1 at the N vacancy in h-BN have the lowest barriers for both dehydrogenation steps. Hence, we predict that Pt and Ru single atoms anchored at vacancy sites in h-BN are promising catalysts for propane dehydrogenation.

Computational Methods

First principles density function theory (DFT) calculations were carried out via Vienna Ab initio Simulation Package (VASP).[39] Spin-polarized calculations were performed with the Perdew, Burke, and Ernzerhof (PBE) exchange-correlation functional.[40] The electron-ion interaction was described by projector augmented wave potentials.[41] The cutoff energy of the plane wave basis set was 400 eV. The Brillouin zone sampling was carried out by using a 3×3×1 k-point mesh for a single layer h-BN with a 4×4 lateral unit cell. A vacuum layer ~20 Å along the c-direction was used in our slab models. For density of states calculation, a 5×5×1 k-point mesh was utilized. Convergence criterion was 0.05 eV/Å for both geometry optimization and transition state search. All atoms were relaxed during geometry optimization.

Single atom anchoring energy was calculated following $E_{SAC} = E_{total} - E_{SA} - E_v$, where E_{total} denotes the total energy of h-BN-supported single atom, E_{SA} the energy of a gas-phase single atom, and E_v the energy of h-BN surface with a B or N vacancy. The climbing-image nudged elastic band (CI-NEB) method[42] was used to search for the transition states. The coordinates for the six SACs explored and the key transitions states are provided in the Supporting Information (SI).

First principles molecular dynamic (FPMD) simulations were performed in 10 ps timescale at constant 1000 K with the NVT ensemble and a time step of 1 fs. The energy drifts of the systems are shown in Figure S1 of SI. Analysis of crystal orbital Hamiltonian populations was carried out using the Local orbital Basis Suite towards Electronic-Structure Reconstruction (LOBSTER) program (version 3.2.0),[43-44] which uses as input the charge density and wavefunction files from VASP calculations.

Acknowledgement

This research was sponsored by the U.S. Department of Energy, Office of Science, Office of Basic Energy Sciences, Chemical Sciences, Geosciences, and Biosciences Division, Catalysis Science Program. This research used resources of the National Energy Research Scientific Computing Center, a DOE Office of Science User Facility supported by the Office of Science of the U.S. Department of Energy under contract no. DE-AC02-05CH11231.

Data Availability

The data that support the findings of this study are available from the corresponding author upon reasonable request.

Supporting Information: energy drift data in FPMD; change of M-B/N bond length after adsorption of C_3H_8.

[1] B. Qiao, A. Wang, X. Yang, L. F. Allard, Z. Jiang, Y. Cui, J. Liu, J. Li, T. Zhang, *Nat. Chem.* **2011**, *3*, 634-641.

[2] D. Wu, W. Chen, X. Wang, X.-Z. Fu, J.-L. Luo, *J. CO2 Util.* **2020**, *37*, 353-359.

[3] M. Hu, Z. Yao, X. Wang, *Ind. Eng. Chem. Res.* **2017**, *56*, 3477-3502.

[4] X. Fan, G. Zhang, F. Zhang, *Chem. Soc. Rev.* **2015**, *44*, 3023-3035.

[5] A. Zitolo, V. Goellner, V. Armel, M.-T. Sougrati, T. Mineva, L. Stievano, E. Fonda, F. Jaouen, *Nat. Mater.* **2015**, *14*, 937-942.

[6] H. Fei, J. Dong, M. J. Arellano-Jiménez, G. Ye, N. Dong Kim, E. L. G. Samuel, Z. Peng, Z. Zhu, F. Qin, J. Bao, M. J. Yacaman, P. M. Ajayan, D. Chen, J. M. Tour, *Nat. Commun.* **2015**, *6*, 8668.
[7] A. M. Love, B. Thomas, S. E. Specht, M. P. Hanrahan, J. M. Venegas, S. P. Burt, J. T. Grant, M. C. Cendejas, W. P. McDermott, A. J. Rossini, I. Hermans, *J. Am. Chem. Soc.* **2019**, *141*, 182-190.
[8] J. T. Grant, C. A. Carrero, F. Goeltl, J. Venegas, P. Mueller, S. P. Burt, S. E. Specht, W. P. McDermott, A. Chieregato, I. Hermans, *Science* **2016**, *354*, 1570-1573.
[9] K. Uosaki, G. Elumalai, H. Noguchi, T. Masuda, A. Lyalin, A. Nakayama, T. Taketsugu, *J. Am. Chem. Soc.* **2014**, *136*, 6542-6545.
[10] C. Jin, F. Lin, K. Suenaga, S. Iijima, *Phys. Rev Lett.* **2009**, *102*, 195505.
[11] W. Zhu, X. Gao, Q. Li, H. Li, Y. Chao, M. Li, S. M. Mahurin, H. Li, H. Zhu, S. Dai, *Angew. Chem. Int. Ed.* **2016**, *55*, 10766-10770.
[12] W. Zhu, Z. Wu, G. S. Foo, X. Gao, M. Zhou, B. Liu, G. M. Veith, P. Wu, K. L. Browning, H. N. Lee, H. Li, S. Dai, H. Zhu, *Nat. Commun.* **2017**, *8*, 15291.
[13] S. Abdel Aal, *Surf. Sci.* **2016**, *644*, 1-12.
[14] K. Mao, L. Li, W. Zhang, Y. Pei, X. C. Zeng, X. Wu, J. Yang, *Sci. Rep.* **2014**, *4*, 5441.
[15] Z. Lu, P. Lv, Y. Liang, D. Ma, Y. Zhang, W. Zhang, X. Yang, Z. Yang, *Phys. Chem. Chem. Phys.* **2016**, *18*, 21865-21870.
[16] S. Lin, X. Ye, R. S. Johnson, H. Guo, *J. Phys. Chem. C* **2013**, *117*, 17319-17326.
[17] C. Huang, X. Ye, C. Chen, S. Lin, D. Xie, *Comput. Theor. Chem.* **2013**, *1011*, 5-10.
[18] P. Zhao, Y. Su, Y. Zhang, S.-J. Li, G. Chen, *Chemical Physics Letters* **2011**, *515*, 159-162.
[19] J. Zhao, Z. Chen, *J. Am. Chem. Soc.* **2017**, *139*, 12480-12487.
[20] C. Deng, R. He, D. Wen, W. Shen, M. Li, *Phys. Chem. Chem. Phys.* **2018**, *20*, 10240-10246.
[21] I. Jiménez, A. Jankowski, L. J. Terminello, J. A. Carlisle, D. G. J. Sutherland, G. L. Doll, J. V. Mantese, W. M. Tong, D. K. Shuh, F. J. Himpsel, *Appl. Phys. Lett.* **1996**, *68*, 2816-2818.
[22] Y. Wang, J. Wang, P. Zheng, C. Sun, J. Luo, X. Xie, *J. Energy Chem.* **2022**, *67*, 451-457.
[23] L. Wang, Y. Wang, C.-W. Zhang, J. Wen, X. Weng, L. Shi, *Catal. Sci. Technol.* **2020**, *10*, 1248-1255.
[24] J. J. Sattler, J. Ruiz-Martinez, E. Santillan-Jimenez, B. M. Weckhuysen, *Chem. Rev.* **2014**, *114*, 10613-10653.
[25] S. A. Bradley, W. Sinkler, D. A. Blom, W. Bigelow, P. M. Voyles, L. F. Allard, *Catal. Lett.* **2012**, *142*, 176-182.
[26] S. Chen, X. Chang, G. Sun, T. Zhang, Y. Xu, Y. Wang, C. Pei, J. Gong, *Chem. Soc. Rev.* **2021**, *50*, 3315-3354.
[27] R. T. Hannagan, G. Giannakakis, R. Réocreux, J. Schumann, J. Finzel, Y. Wang, A. Michaelides, P. Deshlahra, P. Christopher, M. Flytzani-Stephanopoulos, M. Stamatakis, E. C. H. Sykes, *Science* **2021**, *372*, 1444-1447.
[28] L. Qi, M. Babucci, Y. Zhang, A. Lund, L. Liu, J. Li, Y. Chen, A. S. Hoffman, S. R. Bare, Y. Han, B. C. Gates, A. T. Bell, *J. Am. Chem. Soc.* **2021**, *143*, 21364-21378.
[29] X. Sun, P. Han, B. Li, Z. Zhao, *The Journal of Physical Chemistry C* **2018**, *122*, 1570-1576.
[30] Z. Jiang, X. Feng, J. Deng, C. He, M. Douthwaite, Y. Yu, J. Liu, Z. Hao, Z. Zhao, *Adv. Funct. Mater.* **2019**, *29*, 1902041.
[31] M. Moses-DeBusk, M. Yoon, L. F. Allard, D. R. Mullins, Z. Wu, X. Yang, G. Veith, G. M. Stocks, C. K. Narula, *J. Am. Chem. Soc.* **2013**, *135*, 12634-12645.
[32] B. Qiao, J.-X. Liang, A. Wang, C.-Q. Xu, J. Li, T. Zhang, J. J. Liu, *Nano Res.* **2015**, *8*, 2913-2924.
[33] B. Qiao, J.-X. Liang, A. Wang, J. Liu, T. Zhang, *Chin. J. Catal.* **2016**, *37*, 1580-1586.
[34] H. Tao, C. Choi, L.-X. Ding, Z. Jiang, Z. Han, M. Jia, Q. Fan, Y. Gao, H. Wang, A. W. Robertson, S. Hong, Y. Jung, S. Liu, Z. Sun, *Chem.* **2019**, *5*, 204-214.
[35] D. Wang, Q. Li, C. Han, Z. Xing, X. Yang, *Appl. Catal. B* **2019**, *249*, 91-97.
[36] Z. Lian, C. Si, F. Jan, S. Zhi, B. Li, *ACS Catal.* **2021**, *11*, 9279-9292.

[37] W. Tang, E. Sanville, G. Henkelman, *J. Phys. Condens. Matter.* **2009**, *21*, 084204.
[38] M.-L. Yang, Y.-A. Zhu, C. Fan, Z.-J. Sui, D. Chen, X.-G. Zhou, *Phys. Chem. Chem. Phys.* **2011**, *13*, 3257-3267.
[39] G. Kresse, J. Furthmüller, *Phys. Rev. B* **1996**, *54*, 11169-11186.
[40] J. P. Perdew, K. Burke, M. Ernzerhof, *Phys. Rev. Lett.* **1996**, *77*, 3865.
[41] P. E. Blöchl, *Phys. Rev. B* **1994**, *50*, 17953.
[42] G. Henkelman, *J. Chem. Phys.* **2000**, *113*, 9901-9904.
[43] S. Maintz, V. L. Deringer, A. L. Tchougréeff, R. Dronskowski, *J. Comput. Chem.* **2016**, *37*, 1030-1035.
[44] R. Dronskowski, P. E. Bloechl, *The Journal of Physical Chemistry* **1993**, *97*, 8617-8624.

Table of Contents

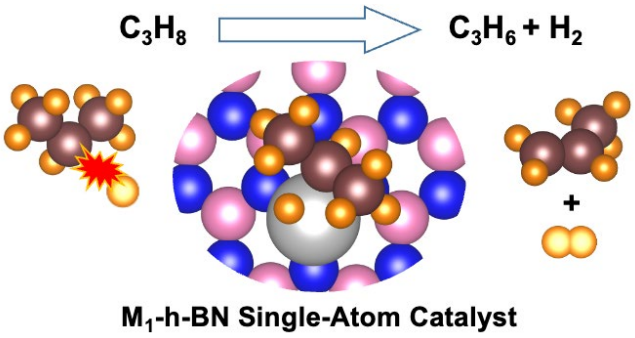

Single-atom catalysis: Pt, Au, and Ru single atoms anchored at B and N vacancies on hexagonal boron nitride are examined with first principles density function theory for their stability and potential for propane dehydrogenation. Pt_1 at the B vacancy in h-BN and Ru_1 at the N vacancy in h-BN are found to be highly stable and active for propane dehydrogenation.